Acta Geotechnica (2020) 15:3307–3320
https://doi.org/10.1007/s11440-020-00956-2

RESEARCH PAPER

Modelling frost heave in unsaturated coarse-grained soils

Jidong Teng[1] · Jianlong Liu[1] · Sheng Zhang[1] · Daichao Sheng[1,2]

Received: 30 July 2019 / Accepted: 16 March 2020 / Published online: 4 April 2020

Abstract

Coarse-grained soils were considered not susceptible to frost heave. However, substantial frost heave has been observed in unsaturated coarse fills in high-speed railway embankments. Recent experimental results in the literature show that vapour transfer has a considerable influence on the frost heaving of coarse-grained soil. However, vapour transfer has rarely been considered in modelling frost heave. This study presents a new frost heave model that considers vapour transfer and its contribution to ice formation. An updated computer program (PCHeave) is developed to account for the vapour transfer in unsaturated coarse-grained soils, where the rigid ice theory is applied to initiate ice lens formation in the frozen fringe. The results of the proposed model are compared with laboratory test results, which show reasonable agreement. The frost heave data monitored in 2013–2014 along the embankment of the Harbin–Dalian Passenger Dedicated Railway are also used to validate the proposed model. The prediction of the model agrees well with the measured results of frost heave and frost depth. This indicates that the proposed model can reasonably reflect the process of frost heave caused by vapour transfer in unsaturated coarse-grained soils.

Keywords Frost heave · Numerical model · Unsaturated coarse-grained soil · Vapour transfer

List of symbols

dx_f/dt	The advancing rate of the frost front x_f or the frost penetration rate during Δt and is negative when frost advances downwards (m/s)
σ	The total stress or the total overburden pressure (Pa)
σ'	The effective stress (Pa)
n	The soil porosity
I	The ice content
$\bar{I}$	Mean ice content in the current frozen fringe
I_b	The current volumetric ice content at x_b
u_w	The pore water pressure (Pa)
u_i	The pore ice pressure (Pa)
u_n	The neutral stress (Pa)
ρ_w	The density of liquid water (g/cm^3)
ρ_i	The density of ice (g/cm^3)
ρ_v	Density of vapour (g/cm^3)
$\bar{\lambda}_f$	Effective thermal conductivity of the layer above x_b (W/(m °C)
$\bar{\lambda}_{ff}$	Effective thermal conductivity of the current frozen fringe (W/(m °C)
$\bar{\lambda}_u$	Effective thermal conductivity of the unfrozen zone between x_f and x_w (Fig. 1) (W/(m °C)
λ_{sat}	Thermal conductivity of a soil saturated by water and ice (W/(m °C)
λ_{dry}	Thermal conductivity of the dry soil (W/(m °C)
x_c	Either the cold boundary of the soil profile for coarse calculation or the location of the cold boundary of the growing ice lens (m)
x_f	Location of the frost front (m)
x_b	Warm surface of the latest ice lens (m)
x_w	Boundary of the soil layer below the frost front (m)
T_0	The freezing point of water in degree Kevin (K)
T_c	Temperature at location x_c (°C)
T_f	Temperature at location x_f (°C)
T_s	Temperature at the ice–water interface or the so-called segregational temperature (°C)
T_w	Temperature at warm side x_w (°C)
V_i	Rate of ice lensing or the rate of heave during the time step Δt (m/s)
L	Specific latent heat of water (J/kg)

✉ Sheng Zhang
zhang-sheng@csu.edu.cn

[1] National Engineering Laboratory for High-Speed-Railway Construction, Central South University, Railway Campus of Central South University, Shaoshan South Road No. 68, Changsha 410075, Hunan Province, China

[2] School of Civil and Environmental Engineering, University of Technology Sydney, Sydney, Australia

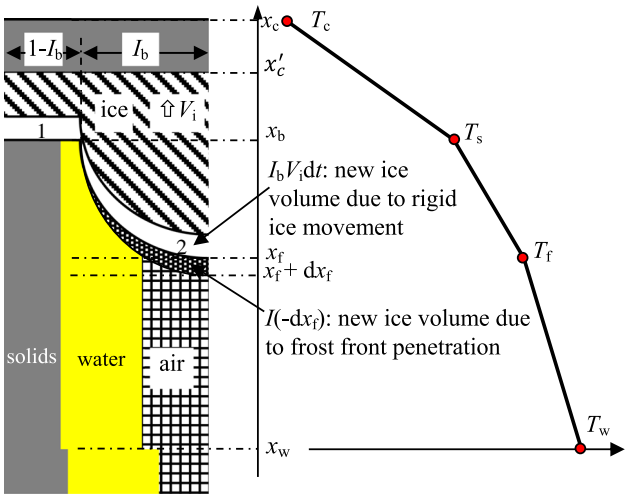

Fig. 1 Phase volumes and temperature profile around the frozen fringe

L_{vap}	Specific latent heat of vapour (J/kg)
s_r	Degree of saturation
v_{ff}	Rate of water flow in the frozen fringe (m/s)
v_u	Rate of water flow at the frost front (in the unfrozen soil) (m/s)
v_{vap}	Vapour flux in the unfrozen zone (m/s)
k_u	Effective hydraulic conductivity of the unfrozen soil between the frost front and the groundwater table (m/s)
g	Acceleration of gravity (m/s^2)
x_{gw}	Location of the groundwater table (m)
$u_w(x_{gw})$	Pore water pressure at the ground water table (Pa)
$u_w(x_f)$	Pore water pressure at the frost front (x_f) (Pa)
Kvh	Thermal vapour hydraulic conductivities
KvT	Thermal vapour hydraulic conductivities
h	The total thickness (m)
h_i	The thickness of the ith layer (m)
Λ_i	The parameter of the ith layer
k	The hydraulic conductivity of unsaturated soil in the unfrozen state (m/s)
k_{sat}	The saturated hydraulic conductivity (m/s)
θ_u	The unfrozen volumetric water content
θ_0	The initial volumetric water content
M	The molecular weight of water (= 0.018) (kg/mol)
R	The universal gas constant (= 8.341) (J/(mol K)
H_r	The dimensionless relative humidity
ρ_{vs}	The saturated vapour density (kg/m^3)
D	The vapour diffusivity in soil (m^2/s)
τ	The tortuosity factor
θ_a	The air-filled porosity
D_a	The diffusivity of water vapour in air (m^2/s)
η	A dimensionless enhancement factor
f_c	The mass fraction of clay content of the soil

1 Introduction

The Harbin–Dalian Passenger Dedicated Railway is the first dedicated passenger line in the world to operate in cold regions. In seasonally frozen soil areas, the effects of frost heave on high-speed railways are significant because of stringent deformation requirement of truck foundation. These coarse fills for high-speed railways, classified as Group A and Group B in the Chinese standard, have low fines contents (typically, $< 10\%$) and very low initial water content (typically, 5% in mass). The groundwater table is located far below the coarse fills. The coarse fills were considered not susceptible to frost heave, but substantial frost heave has been observed in the coarse fills in high-speed railway embankments [29, 30, 45, 46, 54, 55]. Therefore, it is important to explain the unusual phenomenon and predict the frost heave of coarse-grained soils.

A number of theories in the literature have been developed to predict frost heave. Five main streams of the theories can be identified: (1) the capillary theory based on the Young–Laplace equation for primary frost heave [1, 6, 14, 47]; (2) the rigid ice model referred to as the secondary frost heave that assumes the existence of a frozen fringe [2, 10, 27, 28, 31, 33, 42, 43]; (3) the hydrodynamic models or the thermo-hydro-mechanical models [12, 13, 15, 20–22, 24, 53, 56]; (4) the segregation potential models, which are based on the proportional relation between the velocity of water entering the unfrozen soil and the temperature gradient [16–19]; (5) the theory of premelting dynamics that considers the intermolecular forces causing premelted fluid to migrate and supply segregated ice growth and frost heave [36–38, 41].

In all the models and theories discussed above, including the more recent premelted ice model, frost heave is considered to be a consequence of freezing and migration of liquid water in fine grained soil. Indeed, the frozen fringe is assumed to be fully saturated by water and ice, both in the rigid ice model, in the segregational potential theory and in the premelted ice model. According to the above theories, liquid water in coarse-grained soils above the groundwater table is usually discontinuous. It is then difficult for liquid water to flow to the freezing front or the frozen fringe. The frozen fringe in coarse-grained soils such as sand or gravel is very thin or zero [27], which prevents the formation of ice lens. According to existing

models and theories, freezing of a coarse-grained soil does not cause the formation of ice lenses or much frost heave.

The experimental results in the literature show that vapour transfer has an important effect on the frost heave of coarse-grained soil [5, 11, 29, 49]. Teng et al. [50] performed a series of laboratory tests to investigate the factors that will affect vapour transfer in a clean sand, including initial water content, dry density, boundary temperature, and water supply pattern. They found that vapour transfer can be the primary mechanism of moisture migration in coarse-grained soil, especially when the initial water contents of the soils are low. It is found that under sub-freezing temperatures, the liquid water and vapour in the coarse-grained soils can change phase into ice, reducing the humidity and moisture content of the air in the soil. A thin water film exists on the surface of ice crystals in coarse-grained soils, which can generate considerable adsorption potential [4]. This kind of potential increases the matric suction of the soil and reduces the concentration of vapour, thus continuously driving the migration of vapour to the freezing zone [50]. The migration of vapour will support the continuous growing of the ice lens, leading to frost heave in the soils [9, 56]. As the above experimental observations, ice lensing and frost heave can take place in relatively dry soils due to vapour flow, very similar to the ice formation in an old-type freezer. Indeed, any cold surface (with temperature kept below the freezing point of water) exposed to humid air tends to accumulate frost on it. Giving proper conditions and time, the density of the frost can be as high as ice, just as ice stuck to the surface of an old freezer. While the physical process of frost heave in coarse-grained soils is relatively clear and validated by experiments, the corresponding mathematical model is still lacking. It is relatively unknown: how to model frost heave in coarse-grained soils and how much frost heave can form due to vapour transfer.

The objective of this study is to develop a new frost heave model that takes into account the vapour transfer and phase change in coarse-grained soils. The numerical model is described in detail and further implemented into the program PCHeave. The results of the numerical modelling are then compared with laboratory test results and in situ measurement data of the Harbin–Dalian Passenger Dedicated Railway. The results show that the model simulation matches well with the test results. The significance of vapour transfer in coarse-grained soils is analysed based on the proposed model, and finally, some concluding remarks are summarized.

2 Theory

2.1 Basic assumptions

PCHeave is a computer program developed by Sheng [42] and Sheng et al. [43] that can simulate the formation of discrete ice lenses in soil and predict the one-dimensional frost heave. One key feature of the model is that only a small number of soil parameters are involved and all these parameters have physical meaning, such as dry density, initial water content, degree of saturation and saturated hydraulic conductivity [45]. Although PCHeave is one of the few models that can be used to predict frost heave in engineering practice, it cannot explain the frost heave in coarse-grained soil caused by vapour transfer. This study further develops the PCHeave model into a new version to account for the effect of vapour transfer on the accumulation of pore ice. The basic assumptions in the new model are updated as follows:

(a) A frozen fringe is assumed to exist that is always saturated by water or ice. This is in accordance with the rigid ice concept proposed in Miller [27].
(b) The vapour inflow at the freezing front will condense to water and fill the pores of the frozen fringe.
(c) The soil profile is made of an arbitrary number of soil layers.
(d) The temperature gradients in each soil layer are linear, but may vary with time.
(e) The hydraulic conductivity of the frozen fringe decreases exponentially as a function of the temperature.
(f) The rates of water flow in the frozen fringe and in each unfrozen soil layer are constant in space, but may vary with time.
(g) The pore ice particles in the frozen fringe are connected to the warmest ice lens as a rigid body.
(h) The Clapeyron equation is used to describe the pressures and temperature at the water/ice interface.
(i) At any time, there is only one ice lens growing (old ice lenses stop growing once a new ice lens forms).
(j) The rate of frost heave is the same as the rate of ice lens growth.

2.2 Ice lens initiation

There exist a film of unfrozen water between the soil particles and the ice due to the action of surface energy among soil particles. Unfrozen water film is the path for liquid water to flow in the frozen fringe. Due to the existence of the unfrozen water film, the ice pressure and water pressure act around each soil particle in a balanced manner

in the frozen fringe. Since both ice and water phases appear in the frozen fringe, the effective pore pressure is defined as a weighted sum of the ice pressure and water pressure, which represents the difference between the total stress and the effective stress. It is then possible that the effective stress approaches zero at some point in the frozen fringe if the ice pressure is sufficiently high there. Therefore, a new ice lens can form at that point by separating 'floating' soil particles. The mechanism of ice lensing associated with the existence of a frozen fringe is termed the secondary heaving by Miller [25, 26]. Therefore, a new ice lens is assumed to be initiated when and where the effective stress in the soil approaches zero [43, 44]. The effective stress is defined as follows:

$$\sigma' = \sigma - \frac{n-I}{n}u_{\mathrm{w}} - \frac{I}{n}u_{\mathrm{i}} = \sigma - u_{\mathrm{n}} \tag{1}$$

where σ is the total stress or the total overburden pressure, σ' is the effective stress, n is the soil porosity includes the volume of ice, I is the volumetric percentage of ice in the total soil, u_{w} is the pore water pressure, u_{i} is the pore ice pressure, and u_{n} is the neutral stress.

The water pressure at the warm side of the lens, which appears in suction, is affected by the segregational temperature and the overburden pressure, through the Clapeyron equation in thermodynamics. Assuming the ice–water interface is at equilibrium, the ice pressure, water pressure and temperature are related through the integrated Clapeyron equation as follows:

$$\frac{u_{\mathrm{w}}}{\rho_{\mathrm{w}}} - \frac{u_{\mathrm{i}}}{\rho_{\mathrm{i}}} = L\frac{T_{\mathrm{s}}}{T_0} \tag{2}$$

where ρ_{w} is the density of liquid water, ρ_{i} is the density of ice, L is the specific latent heat of water, T_0 is the freezing point of water in degree Kevin, T_{s} is the temperature at the ice–water interface or the so-called segregational temperature [52]. Ice segregation temperature T_{s} is defined as temperature at the position of warm surface of the latest ice lens, i.e. warm end of segregation ice layer. It is related to the principle of water migration and both of ice and unfrozen water equilibrium. The approximation T_{s} can be obtained by the curve of unfrozen water content versus temperature.

Substituting Eq. (2) into Eq. (1) to eliminate the ice pressure leads to the following:

$$u_{\mathrm{n}} = \left(1 - \frac{I}{n} + \frac{I}{n}\frac{\rho_{\mathrm{i}}}{\rho_w}\right)u_{\mathrm{w}} - L\rho_{\mathrm{i}}\frac{I}{n}\frac{T_{\mathrm{s}}}{T_0} \tag{3}$$

A new ice lens is initiated within the frozen fringe when and where the neutral stress reaches the total stress or the total overburden pressure. The neutral stress can be determined by Eq. (3).

2.3 Heat and mass transfer

Assume the location of the frozen fringe is known at the time t. The aim is to determine the rate of heave during a small-time step Δt and the new location of the frozen fringe at time $t + \Delta t$.

The volumetric ice content is 1 above x_{b}, I_{b} (not necessarily equal 1) at x_{b} and zero at x_{f}, as shown in Fig. 1. The x_{b} is the warm surface of the latest ice lens, and x_{f} is the location of the frost front. The parameter $\bar{I}$ is the average ice content in the frozen fringe. It is noted that porosity n includes the volume of ice. Therefore, if the rigid ice body moves upwards at a velocity V_{i}, a space of the size $(1V_{\mathrm{i}}\mathrm{d}t)$ will be left during time period $\mathrm{d}t$ and must be filled by new formed ice, which includes the ice formed at x_{b}, i.e. $I_{\mathrm{b}}V_{\mathrm{i}}\mathrm{d}t$, and that within the fringe, i.e. $(1 - I_{\mathrm{b}})V_{\mathrm{i}}\mathrm{d}t$. In addition, the penetration of the frost front $(-\mathrm{d}x_{\mathrm{f}})$ will also cause an ice formation of the volume of $\bar{I}(-\mathrm{d}x_{\mathrm{f}})$.

As shown in Fig. 1, the white area 1 represents the ice formed within the fringe, i.e. $(1 - I_{\mathrm{b}})V_{\mathrm{i}}\mathrm{d}t$. The white area 2 represents the ice formed at x_{b}, i.e. $I_{\mathrm{b}}V_{\mathrm{i}}\mathrm{d}t$. The grey area between x_{c} and x_{c}' represents frozen soil, which includes soil particles, ice lens and unfrozen water. The x_{c}' is the colder side of an ice lens, while the x_{w} is the boundary of a soil layer below the frost front. The dislocation at x_{w} is to represent the difference in different soil layers.

The heat balance is considered for each soil layer. At the warm surface of the latest ice lens (x_{b} in Fig. 1), the heat balance states the following:

$$\bar{\lambda}_{\mathrm{f}}\frac{T_{\mathrm{s}} - T_{\mathrm{c}}}{x_{\mathrm{c}} - x_{\mathrm{b}}} - \bar{\lambda}_{\mathrm{ff}}\frac{T_{\mathrm{f}} - T_s}{x_{\mathrm{b}} - x_{\mathrm{f}}} = (1 - I_{\mathrm{b}})V_{\mathrm{i}}\rho_{\mathrm{i}}L \tag{4}$$

where $\bar{\lambda}_{\mathrm{f}}$ is the effective thermal conductivity of the layer above x_{b}, $\bar{\lambda}_{\mathrm{ff}}$ is the effective thermal conductivity of the current frozen fringe, x_{c} is either the cold boundary of the soil profile for coarse calculation or the location of the cold boundary of the growing ice lens, T_{c} is the temperature at location x_{c}, T_{f} is the temperature at location x_{f}, I_{b} is the current volumetric ice content at x_{b}, and V_{i} is the rate of ice lensing or the rate of heave during the time step Δt.

The overall heat balance for the frozen fringe can be expressed as follows:

$$\bar{\lambda}_{\mathrm{f}}\frac{T_{\mathrm{s}} - T_{\mathrm{c}}}{x_{\mathrm{c}} - x_{\mathrm{b}}} - \bar{\lambda}_{\mathrm{u}}\frac{T_{\mathrm{w}} - T_{\mathrm{f}}}{x_{\mathrm{f}} - x_{\mathrm{w}}} = \left(V_{\mathrm{i}} + \bar{I}\left(-\frac{\mathrm{d}x_{\mathrm{f}}}{\mathrm{d}t}\right)\right)\rho_{\mathrm{i}}L + \left(n(1 - S_{\mathrm{r}})\left(-\frac{\mathrm{d}x_{\mathrm{f}}}{\mathrm{d}t}\right)\right)\rho_{\mathrm{w}}L_{\mathrm{vap}} \tag{5}$$

where $\mathrm{d}x_{\mathrm{f}}/\mathrm{d}t$ is the advancing rate of the frost front x_{f} or the frost penetration rate during Δt and is negative when frost advances downwards, $\bar{\lambda}_{\mathrm{u}}$ is the effective thermal conductivity of the unfrozen zone between x_{f} and x_{w} (Fig. 1), T_{w} is

the temperature at warm side x_w, s_r is the degree of saturation, and L_{vap} is the specific latent heat of vapour. The first term on the right-hand side represents the latent heat for the new ice mass formed in the frozen fringe. The second term represents the latent heat for the new liquid water formed in the frozen fringe. The unfrozen soil is unsaturated, but the frozen fringe is saturated. So, the vapour inflow at the frost front will condense to water and fill the pores of frozen fringe.

The mass conservation at x_b requires that the water flow to x_b equals the ice mass formed there:

$$v_{ff}\rho_w = (1 - I_b)V_i\rho_i \tag{6}$$

where v_{ff} denotes the rate of water flow in the frozen fringe.

The overall mass balance within the frozen fringe requires that the outflow of ice mass at x_b must balance the inflow of water mass at x_f plus the mass loss in the frozen fringe as follows:

$$\begin{aligned} V_i\rho_i = {} & v_u\rho_w + (\rho_w - \rho_i)\bar{I}\left(-\frac{dx_f}{dt}\right) \\ & - (\rho_w n(1 - S_r))\left(-\frac{dx_f}{dt}\right) \end{aligned} \tag{7}$$

where v_u is the rate of water flow at the frost front (in the unfrozen soil). The second term on the right-hand side is the mass loss due to phase change, and the third term is the water mass needed to fill the initially unsaturated soil.

In the case where the frost front is above the groundwater table, the rate of water flow in the unfrozen soil (v_u) can be determined from Darcy's law as follows:

$$v_u = \frac{k_u}{\rho_w g}\left(\frac{u_w(x_{gw}) - u_w(x_f)}{x_f - x_{gw}} - \rho_w g\right) + \frac{\rho_v}{\rho_w}v_{vap} \tag{8}$$

where k_u is the effective hydraulic conductivity of the unfrozen soil between the frost front and the groundwater table, g is the acceleration of gravity, x_{gw} is the location of the groundwater table, $u_w(x_{gw})$ is the pore water pressure at the ground water table, $u_w(x_f)$ is the pore water pressure at the frost front (x_f), and v_{vap} is the vapour flux in the unfrozen zone. The pore water pressure at the groundwater table is usually zero, unless an excess pore pressure is considered.

According to the previous studies [3, 8, 34, 35, 40, 48, 56, 57], temperature and vapour pressure gradient (relative humidity) are the two main driving mechanisms for vapour transfer in unsaturated soil. The vapour flux in unsaturated soils can be quantitatively described by Fick's law, as follows:

$$\frac{\rho_v}{\rho_w}v_{vap} = \frac{k_{vh}}{\rho_w g}\left(\frac{u_w(x_{gw}) - u_w(x_f)}{x_f - x_{gw}}\right) + k_{vT}\frac{T_w - T_f}{x_f - x_w} \tag{9}$$

where K_{vh} and k_{vT} are the isothermal and thermal vapour hydraulic conductivities, respectively. The calculation of the two vapour 'permeabilities' is given below.

If the water flow rate in the frozen fringe (v_{ff}) is assumed to be constant, the pore water pressure in the frozen fringe can be found by integrating from Darcy's law, with the assumed hydraulic conductivity function as follows:

$$v_{ff} = -\frac{k_{ff}}{\rho_w g}\left(\frac{du_w}{dx} + \rho_w g\right) \tag{10}$$

$$k_{ff} = k_u \exp(-b(x - x_f)) \tag{11}$$

Substituting Eq. (11) into Eq. (10) to eliminate k_{ff}, and integrating for u_w leads to the following:

$$u_w(x) = -v_{ff}\rho_w g\frac{\exp(b(x - x_f))}{bk_u} - \rho_w g x + C \tag{12}$$

The integration constant C can be determined from the boundary values at x_b, where the pore water pressure is related to the pore ice pressure (overburden) and the temperature via the generalised Clapeyron equation as follows:

$$\begin{aligned} u_w(x) = {} & L\rho_w\frac{T_s}{T_0} + \sigma\frac{\rho_w}{\rho_i} \\ & + v_{ff}\rho_w g\frac{\exp(bx_b - bx_f) - \exp(bx - bx_f)}{bk_u} \\ & + \rho_w g(x_b - x) \end{aligned} \tag{13}$$

where σ is the overburden pressure at location x_b, k_u is the saturated hydraulic conductivity of the soil with in the frozen fringe (before freezing), and b is a parameter that will be determined below. The pore water pressure at the position of x_b and x_f can be given as follows:

$$u_w(x_b) = L\rho_w\frac{T_s}{T_0} + \sigma\frac{\rho_w}{\rho_i} \tag{14a}$$

$$\begin{aligned} u_w(x_f) = {} & L\rho_w\frac{T_s}{T_0} + \sigma\frac{\rho_w}{\rho_i} + v_{ff}\rho_w g\frac{\exp(bx_b - bx_f) - 1}{bk_u} \\ & + \rho_w g(x_b - x_f) \end{aligned} \tag{14b}$$

$$\text{Note}: \exp(bx_b - bx_f) = \frac{k_{ff}(x_f)}{k_{ff}(x_b)} \tag{14c}$$

Equations (4)–(14) form the basis of the frost heave model. Providing the location of the frozen fringe (x_f, x_b), the ice content (I) within the frozen fringe and the material parameters involved are known, and they can be solved by iteration for the six unknowns T_s, V_i, dx_f/dt, v_{ff}, v_u and $u_w(x)$.

If the frost front penetrates below the groundwater table, the pore water pressure at the frost front is then determined by the following:

$$u_w(x_f) = (x_{gw} - x_f)\rho_w g \tag{15}$$

In this case, Eqs. (4), (5), (6) and (13) are still valid. Together with Eq. (15), the five equations are solved for the five unknowns T_s, V_i, dx_f/dt, v_{ff} and $u_w(x)$.

2.4 Steady state of growth

In the case where the frozen fringe is too thin for computational significance, the base of the latest ice lens is set to the frost front. The rate of water flow in the unfrozen zone is then in equilibrium with the rate of ice lensing; thus, the frost front will remain stationary. The following equation is used instead of Eqs. (4) and (5)

$$\bar{\lambda}_f \frac{T_s - T_c}{x_c - x_b} - \bar{\lambda}_u \frac{T_w - T_s}{x_b} = V_i \rho_i L \tag{16}$$

The following mass balance equation is used instead of Eqs. (6–7):

$$v_u \rho_w = V_i \rho_i \tag{17}$$

Equations (8) and (13) are still valid. Together with Eqs. (16) and (19), the four equations can be solved for the four unknowns: T_s, V_i, v_u, and $u_w(x)$.

So far, the governing equations have been established based on knowledge of the location of the frozen fringe. The next step is to locate the frozen fringe at each time step. If the frozen fringe (x_f, x_b) is known at time t, the frost penetration rate dx_f/dt can be determined and the new position of the frost front at time $t + \Delta t$ is $x_f + (dx_f/dt)\Delta t$. The position of the warm surface of the latest ice lens x_b remains fixed unless a new ice lens appears within the frozen fringe. A new ice lens appears when and where the effective stress vanishes.

2.5 Material properties

The governing equations contain a number of material parameters that must be determined. Such parameters include the effective thermal conductivity and the hydraulic conductivity of a multi-layer structure, the thermal conductivity and the hydraulic conductivity of a multi-phase material, and the ice content of the frozen fringe.

The effective value of a conductive parameter of a stratified profile, *e.g.* the effective thermal conductivity and the effective hydraulic conductivity, can be represented by the harmonic mean as follows:

$$\bar{\Lambda} = \frac{h}{\left(\frac{h_1}{\Lambda_1} + \frac{h_2}{\Lambda_2} + \cdots\right)} \tag{18}$$

where $\bar{\Lambda}$ denotes the effective value to be determined, h is the total thickness, h_i is the thickness of the ith layer, and i is the parameter of the ith layer.

In the frozen zone, frozen soil is interlayered with pure ice lenses. The equivalent thermal conductivity can be calculated in a manner analogous to the resistance in a series electrical circuit, i.e., using a harmonic mean as follows:

$$\bar{\lambda}_f = \frac{h - x_b}{\frac{h-h_0}{\lambda_i} + \frac{h_0 - x_b}{\lambda_f}} \tag{19}$$

The thermal conductivity of a soil saturated by water and ice can be expressed by the geometric mean as follows:

$$\lambda_{sat} = \lambda_s^{1-n} \lambda_w^{n-I} \lambda_i^I \tag{20}$$

where subscripts s, w and i stand for soil solids, water and ice, respectively.

The thermal conductivity of an unsaturated soil is given as:

$$\lambda = \left(\lambda_{sat} - \lambda_{dry}\right) K_e + \lambda_{dry} \tag{21}$$

where λ_{dry} is the thermal conductivity of the dry soil, and K_e a parameter called the Kersten number [7].

The hydraulic conductivity of a partially frozen soil is a function of the temperature and the soil. The specific function used here is as follows:

$$k_{ff} = k_u \exp(cT - cT_f) = k_u \exp(-bx + bx_f) \tag{22}$$

The parameter b in Eq. (22) can either be treated as an input parameter or, as a first approximation, be estimated as follows:

$$k_{ff} = k_u \left(\frac{\theta_u(x_b)}{n}\right)^9 = k_u \left(\frac{n - I_b}{n}\right)^9 \tag{23}$$

where θ_u is the unfrozen volumetric water content, and the parameter b can be determined by substituting Eq. (23) into Eq. (22) with $x = x_b$ as follows:

$$b = \frac{9 \ln\left(\frac{n-I_b}{n}\right)}{x_f - x_b} = \frac{\ln\left(\frac{k_{ff}(x_b)}{k_{ff}(x_f)}\right)}{x_f - x_b} \tag{24}$$

The hydraulic conductivity of a partially saturated soil in the unfrozen state can be approximated by a given saturated hydraulic conductivity as follows:

$$k = k_{sat} S_r^m \tag{25}$$

where k_{sat} is the saturated hydraulic conductivity and m is a soil parameter and a default value of 9 is used in PCHeave, in accordance with Eq. (23).

The volumetric ice content (I) in the frozen fringe is the difference between the porosity (n) and the unfrozen volumetric water content (θ_u). The unfrozen water content is a function of the temperature or a function of the pressure difference ($u_w - u_i$). The following function is used in PCHeave:

$$I = n - \theta_u(T) = n - \theta_0 \exp\left(\alpha T^{\beta}\right) \tag{26}$$

where θ_0 is the initial volumetric water content and α and β are two constants depending on the specific surface area and pore geometry of the soil. The constant β is approximately 2 for most soils of interest. The constant α can be determined by substituting into Eq. (23) an unfrozen water content at a sub-freezing temperature, e.g.—1.0 °C.

The vapour permeabilities in Eq. (9) can be estimated as follows [57]:

$$k_{vh} = \frac{D}{\rho_w}\left(\rho_{vs}\frac{Mg}{RT}H_r\right) = \frac{D}{\rho_w}\left(\rho_{vs}\frac{Mg}{RT}\exp\left(\frac{u_w(0.5x_f)M}{\rho_w RT}\right)\right) \tag{27}$$

$$k_{vT} = \frac{D}{\rho_w}\eta H_r\left(\frac{d\rho_{vs}}{dT}\right) = \frac{D}{\rho_w}\eta\left(\frac{d\rho_{vs}}{dT}\right)\exp\left(\frac{u_w(0.5x_f)M}{\rho_w RT}\right) \tag{28}$$

where M is the molecular weight of water (= 0.018 kg/mol); R is the universal gas constant (= 8.341 J/(mol K)); and H_r is the dimensionless relative humidity and its expression is given as [39]:

$$H_r = \exp\left(\frac{u_w(0.5x_f)M}{\rho_w RT}\right) \tag{29}$$

In the equation above, ρ_{vs} is the saturated vapour density (kg/m^3), which is an exponential function of temperature, and its expression is given as:

$$\rho_{vs} = \exp(19.84 - 4975.9/T) \times 10^{-3} \tag{30}$$

D in Eqs. (27) and (28) is the vapour diffusivity in soil (m^2/s), which can be obtained by experiments. Nyameogo et al. [32] developed a laboratory method to evaluate the gas diffusion coefficient in frozen soils. It also can be derived from the diffusivity of water vapour in air, as follows:

$$D = \tau\theta_a D_a = (1 - S_r)^2\theta_a^{4/3}D_a = (1 - S_r)^{10/3}n^{4/3}D_a \tag{31}$$

In Eq. (31), τ is the tortuosity factor, θ_a is the air-filled porosity (m^3/m^3 or %), D_a is the diffusivity of water vapour in air (m^2/s), $D_a = 2.12 \times 10^{-5}(T/273.15)^2$, and η is a dimensionless enhancement factor and its expression is given as follows:

$$\eta = 9.5 + 3S_r - 8.5\left(1/\exp\left(1 + 2.6(f_c)^{-0.5}S_r\right)^4\right) \tag{32}$$

In the equation above, f_c is the mass fraction of the clay content of the soil.

All temperatures T are estimated at $0.5x_f$ and in degrees Kevin, i.e. $T = (T_f + T_w)/2 + 273.15$.

2.6 Computation strategy

With Eqs. (18–32), the material parameters used in PCHeave are greatly simplified. The final parameters used in PCHeave include the bottom position of the soil layer, the thermal conductivity of the soil solids, the water content by dry weight, the dry density, the degree of saturation, the saturated hydraulic conductivity and the unfrozen water content at − 1 °C (in percentage of the initial water content). The thermal conductivity of soil solids is approximately 2 ∼ 3 W/mK, and the actual thermal conductivity of a soil is calculated according to Eqs. (18–21). This parameter is kept as an input so that non-soil materials such as insulation, snow and concrete can also be simulated in PCHeave.

In addition to the material parameters, the boundary conditions, groundwater table, external load and geometric make-up of the soil profile must also be specified. The general input parameters in PCHeave include the number of material layers, the total depth of the soil profile, the number of temperature intervals at the cold and warm boundaries, the overburden pressure at the ground surface, the distance to the groundwater table from the ground surface, the total time length and the time step. The temperatures at the cold and warm boundaries can be specified step-wise in a number of intervals. The overburden pressure is the extra load applied at the cold boundary. The soil self-weight is calculated automatically in PCHeave. The size of the time step can affect the results, but the solution converges as the step size is sufficiently small. As the computation in PCHeave is extremely fast (usually in seconds), an appropriate step size can be found by trial and error.

The calculation procedure in PCHeave is illustrated in Fig. 2. The position of the first ice lens is determined

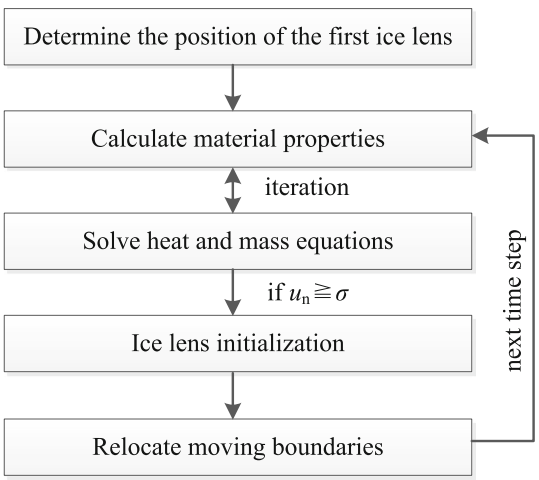

Fig. 2 Calculation procedure in PCHeave

according to the theory discussed in the section location of the frozen fringe. The heat and mass balance Eqs. (4)–(10) are then solved by iteration, for T_s, V_i, dx_f/dt, and $u_w(x)$. The length of the soil column is elongated by $V_i\Delta t$. The frost front moves $(-dx_f/dt)\Delta t$ downwards. The position of the new frozen fringe is determined according to the ice lens formation criterion described by Eqs. (1–3). The system is then ready for the next time step.

3 Model validation and application

3.1 Experimental verification

A series of one-side freezing experiments of a coarse-grained soil were conducted by Gao et al. [9], to test the effect of vapour transfer on the frost heave of a coarse-grained soil. Graded crushed stones containing 5% fines by weight are adopted as the test material. The non-uniformity coefficient of the cumulative curve of the test material is 15.78, and the coefficient of curvature is 2.63, which indicates that the test material belongs to a well-graded soil. The soil specimen is 198 mm in diameter and 200 mm in height. The dry density is controlled at 2.087 g/cm^3, and the initial water content by weight is 8%. During the whole tests progress, no-pressure water supplement was performed. The top temperatures and the bottom temperatures are kept constant at − 12 °C and 2 °C, respectively. The sidewall of the sample is wrapped with thermal insulation material to achieve a unidirectional freezing state from top to bottom. The test period is 12 days. The experimental results are used to validate the proposed model in PCHeave.

In addition, the saturated hydraulic conductivity can be obtained through experiments. The unfrozen water content can be determined by the laboratory test, such as NMR test [51]. There are a large body of previous studies to investigate the unfrozen water content. For sand, the unfrozen water content at − 1 °C (in percentage of initial water content) should be 0–20%. In this study, it is referred to the input value in Sheng et al. [46]. This value is also reasonable according to the test result in Teng et al. [52]. The material parameters, the general input parameters and the boundary temperature specification in PCHeave are given in Table 1.

Figure 3 shows the predicted results of the frost depth and frost heave compared with the measured result in the one-dimensional freezing test. The predicted results without considering vapour transfer are generated by the original model in PCHeave, while the results of considering vapour transfer are computed by the proposed model. The predicted frost depth and frost heave after 288 h are 183 mm and 5.2 mm, respectively, while the measured values for them are 181 mm and 5.5 mm, respectively. The predicted results of the proposed model agree well with the measured data. When using the original model of PCHeave, the predicted frost heave is 1.9 mm after the test, which is considerably less than the measured result of 5.5 mm. This finding is consistent with the results of Zhang et al. [57] that the contribution of vapour flow to total water flux can be significant in the unsaturated freezing coarse soils. It also highlights the importance of vapour transfer in modelling frost heave in coarse-grained soils. The predicted frost depth by the original PCHeave model shows a faster descending rate compared to the experimental values, which may be caused by neglecting the vapour transfer. Phase change from vapour into ice is an exothermic process, and can delay the descent of the freezing front.

The updated PCHeave code can simulate ice lens formation in soils. Figure 4a presents the forms of ice lenses at different times when considering vapour transfer, and Fig. 4b presents the simulated result without considering vapour transfer. Figure 4a shows that a few ice lenses are distributed in the frozen zone of the soil specimen, and the thickest ice lenses occur near the final freezing front. However, if the vapour transfer is neglected, the ice lens only occurs at the position of the freezing front, and there are no ice lenses at the other positions. The reason is that the liquid water at the bottom of the sample can hardly move upward, while vapour will flow upwards driven by the temperature and humidity gradients. As the hydraulic conductivity of the soil close to the ice lens decreases and the freezing front moves downwards, the ice lens will generate at other positions.

3.2 Application to a railway subgrade

To perform a long-term test of the proposed model and evaluate its numerical stability, the updated PCHeave is applied to analyse the in situ monitored results and reveal the frost heave in a subgrade of high-speed railway. The in situ test was performed by Niu et al. [29] to measure the ground temperatures, moisture content, and frost heave of the subgrade of the Harbin–Dalian Passenger Dedicated Line (HDPDL). The subgrade at one site (K977) is built on the undisturbed ground surface, while the other is in a cut section (K1004). Displacement measurements indicate that frost heave at the K977 and K1004 sites increases rapidly to 14 mm and 25 mm, respectively, in 1 month.

The subgrade structure and the measured methods are shown in Fig. 5. The upper layer is a 70-cm-thick well-graded gravel with cement. The middle layer is 230 cm of group A/B fills. The lower layer is a 50-cm-thick well-graded crushed-stone and sand. The group A/B fills belong to high-quality and good filling materials in the China

Table 1 Input parameters in PCHeave for simulating laboratory test

Category	Input parameters	Units	Values
Material Parameters	Bottom position of the soil layer	cm	20
	Thermal conductivity of soil solids	W/mK	3
	Water content by dry weight	%	8
	Dry density	t/m^3	2.087
	Degree of saturation	%	50%
	Saturated hydraulic conductivity	10^{-6} m/s	200
	Unfrozen water content at − 1 °C (in percentage of initial water content)	%	16
General input parameters	Number of material layers	Unitless	1
	Total depth of the soil profile	cm	20
	Number of temperature intervals at the cold boundary	Unitless	1
	Number of temperature intervals at the warm boundary	Unitless	1
	Overburden pressure at the ground surface	kPa	0
	Groundwater table from the ground surface	cm	300
	Total time length	hour	288
	Time step used in the computation	second	100
Boundary temperature specification	Ending time of the interval	hour	288
	Cold temperature in the interval	°C	− 12
	Warm temperature in the interval	°C	2

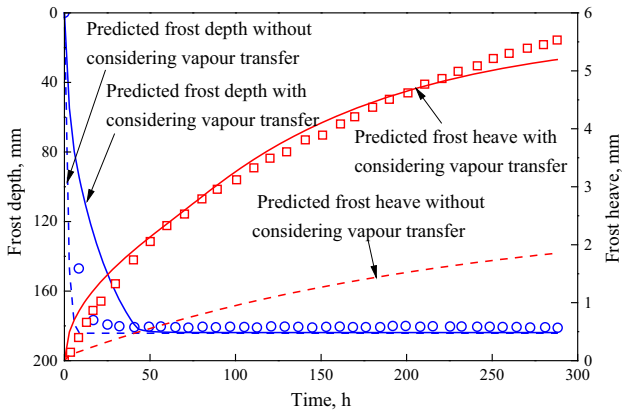

Fig. 3 Comparison between predicted and measured results of frost heave and frost depth. The solid lines are the predicted results by the proposed model, while the dashed lines are the predicted results by the original model in PCHeave. The symbols indicate the measured results

railway construction code. The group A fill materials consist of crushed rock with less than 15% fines content, while the group B materials have fines fractions of 15–30%. The in situ water content of the fills is between 3 and 15% in mass. The original groundwater table is located at a depth of 600 cm.

In this numerical simulation, the soil profile in the subgrade is simplified by considering an embankment of 300 cm height, including the 70 cm cemented gravel at the top. The role of geomembrane is not considered specifically. The reason can be as follows: (1) The 20 cm sand interlayered with a geomembrane is not used everywhere, and this simplification will likely lead to be worse compared to the actual case. (2) The geomembrane at the area of the monitored site has been damaged due to the installation of the data measurement system [29]. And this simplification is consistent with the simulation in Zhang et al. [55].

The main differences between the in situ measurement and the laboratory column experiment are that the amplitude of the upper boundary temperatures is much higher and that the properties of the material are relatively complex and uncertain. The inputs in PCHeave, including soil properties and boundary conditions, are shown in Table 2. Layer 1 is a well-graded gravel with cement and is of 70 cm thickness, while Layer 2 is group A/B fills of 230 cm in thickness. Some input parameters used in PCHeave are determined from the measured values. For example, the initial water contents are assigned to be 4% and 8% for layer 1 and layer 2, respectively, at the K977 site, which are given by averaging the measured values in these two layers. Using the same method, the initial water contents are 5% and 9% for layer 1 and layer 2, respectively, at the K1004 site. The input boundary temperatures are simplified to a constant value by using the harmonic mean method, based on the ground temperature regime in Niu et al. [29]. The top and bottom boundary temperatures at the K977 site are kept constant at − 8 °C and 10 °C, respectively. They are − 9 °C and 10 °C at the

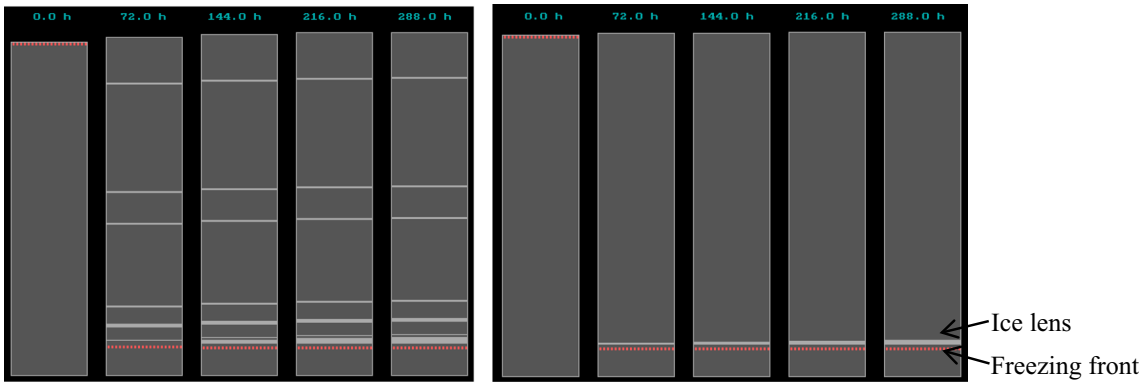

Fig. 4 Simulated ice lens formation in soil specimen

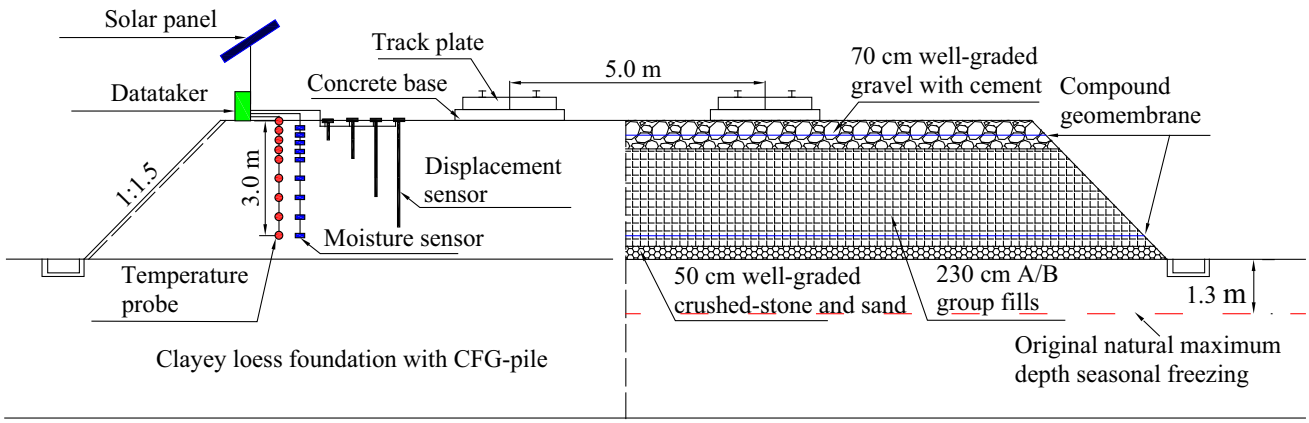

Fig. 5 Embankment structure of the HDPDL and installation of temperature, moisture, and frost heave displacement sensors (after Niu et al. [29]

K1004 site. The overburden pressure is assumed 0. The material parameters, such as dry density, degree of saturation, and saturated hydraulic conductivity, are obtained based on the measured results and the typical values of the related soils [23, 46].

Figure 6 shows the predicted frost depth and frost heave at the K977 site, compared to the measured results by Niu et al. [29]. The result without considering vapour transfer is computed by the original version of PCHeave, and the result of considering vapour transfer is computed by the proposed model in the updated PCHeave. If the vapour transfer is considered in the computation, the predicted frost heave shows good agreement with the measured values. The predicted maximum frost heave in 720 h is approximately 13.0 mm, which is close to the measured values of 13.1 mm. The predicted frost heave has a relatively poorer match with the measured values in the first 600 h. It may be caused by the differences in assumed boundary conditions, such as the constant input boundary temperature and the 0 overburden pressure. Actually, there is a thawing and freezing cycle at the beginning of winter and the dynamic load of the train at ground surfaces. The results of frost heave tests showed that the amount of frost heave caused by the boundary temperature decreased in steps is more than that caused by a constant boundary temperature [45, 50]. Therefore, the simulated frost heave may be underestimated due to the simplified constant boundary temperature. However, overburden pressure can restrain the frost heave. The simulated frost heave may be overestimated due to the assumed 0 overburden pressures. This may be the reason that the predicted maximum frost heave is so close to the measured values. The predicted frost depth agrees well with the measured value in the simulation. The results show that the proposed model performs in simulating unusual frost heave in coarse-grained soils. When using the original PCHeave to make computations, it is found that the predicted frost heave is much lower than the measured values. Only forty percent of the frost heave is obtained by using the original PCHeave, which indicates that the vapour transfer occupies approximately 60% of the total water flux.

Ice lenses formed in the subgrade are simulated by the original and updated PCHeave, and the results are shown in Fig. 7. The computed results in Fig. 7a show that the ice

Table 2 Input parameters in PCHeave for simulating in situ measurements

Category	Input parameters	Units	K977 site		K1004 site	
			Layer 1	Layer 2	Layer 1	Layer 2
Material parameters	Bottom position of the soil layer	cm	70	300	70	300
	Thermal conductivity of soil solids	W/mK	3	3	3	3
	Water content by dry weight	%	4	8	5	9
	Dry density	t/m^3	2.2	2.0	2.2	2.0
	Degree of saturation	%	35	60	40	65
	Saturated hydraulic conductivity	10^{-6} m/s	10	100	10	100
	Unfrozen water content at − 1 °C (in percentage of initial water content)	%	10	16	10	15
General input parameters	Number of material layers	Unitless	2	2		
	Total depth of the soil profile	cm	300	300		
	Number of temperature intervals at the cold boundary	Unitless	1	1		
	Number of temperature intervals at the warm boundary	Unitless	1	1		
	Overburden pressure at the ground surface	kPa	0	0		
	Groundwater table from the ground surface	cm	600	600		
	Total time length	hour	720	1008		
	Time step used in the computation	second	100	100		
Boundary temperature specification	Ending time of the interval	hour	720	1008		
	Cold temperature in the interval	°C	− 8	− 9		
	Warm temperature in the interval	°C	10	10		

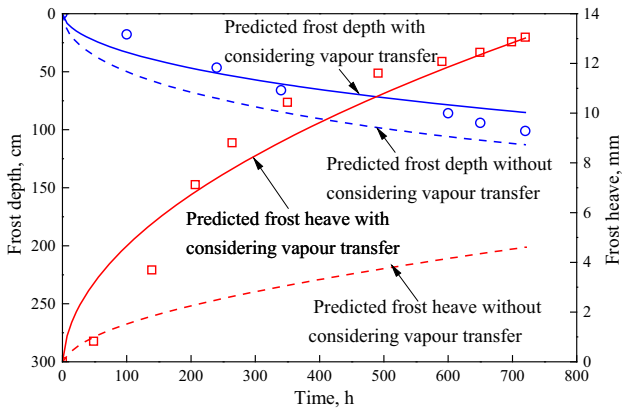

Fig. 6 Comparison between predicted and in situ measured values of frost heave and frost depth at site K977. The solid lines are the predicted result by the proposed model, while the dashed lines are the predicted result by the original model in PCHeave. The symbols indicate the measured results

lens is mainly distributed in the top 70 cm, the closer to the top surface, the thicker the ice lens. It is in accordance with the monitored result that frost heave mainly occurs in the top 60 cm zone. The predicted result in Fig. 7b shows that the ice lenses distributed at depths between 70 and 112 cm, which has some deviation from the field measurements.

Figure 8 shows the predicted frost depth and frost heave at the K1004 site compared to the measured results. The predicted frost heave when considering vapour transfer has good agreement with the measured values. The computed maximum frost heave in 1008 h is approximately 19.1 mm, which is close to the measured 19.5 mm. However, in the first 800 h the predicted frost heave also has a relatively poorer match with the measured values, which may be caused by the input of an averaged boundary temperature and the 0 overburden pressure. It is also found that the predicted frost heave without considering vapour transfer is largely lower than the measured values, which occupies approximately only 40% of the measured frost heave. This indicates that the vapour transfer occupies approximately 60% of the total water flux. The predicted frost depth when considering vapour transfer is always lower than that without considering vapour transfer. The reason is that vapour–ice desublimation is an exothermic process, and the generated heat limits the development of the freezing front. The measured frost depth is somewhere between these two predicted results. The results indicate that the vapour transfer should be taken into account in modelling frost heave in unsaturated coarse-grained soils.

The ice lenses formed at different times at the K1004 site simulated by PCHeave are shown in Fig. 9. As shown

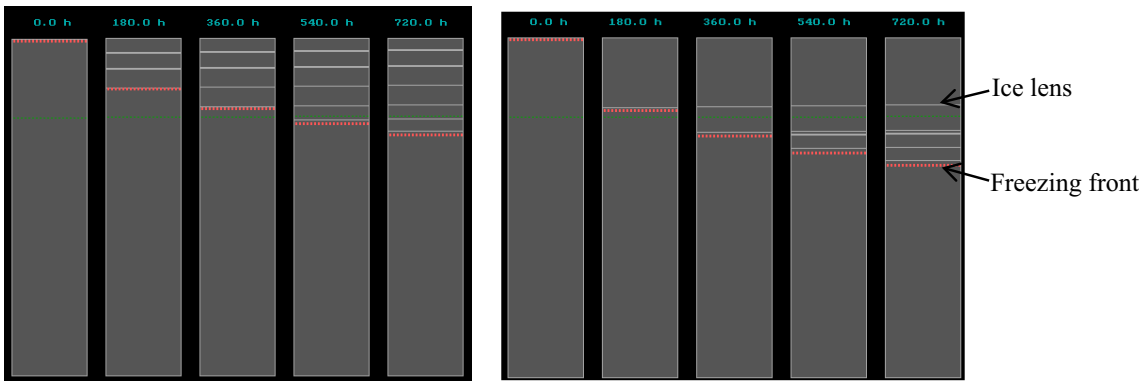

(a) considering vapour transfer **(b)** without considering vapour transfer

Fig. 7 Simulated ice lens formation in subgrade at site K977

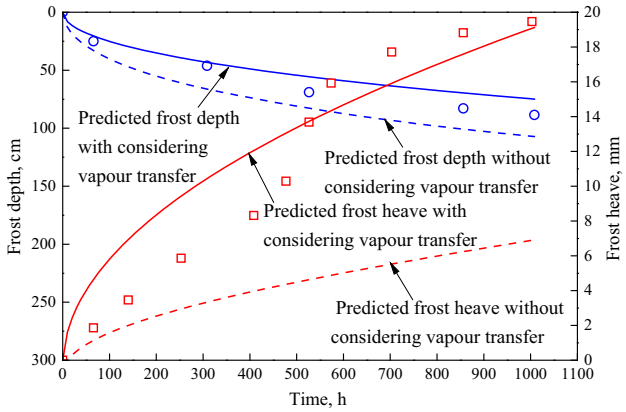

Fig. 8 Comparison between predicted and in situ measured values of frost heave and frost depth at site K1004. The solid lines are the predicted result by the proposed model, while the dashed lines are the predicted result by the original model in PCHeave. The symbols indicate the measured results

in Fig. 9a, ice lenses occur between the top surface and 70 cm depth. This is consistent with the measured results at K977 and is also approximately the same as the monitored results that the ice distributed in the top 60 cm zone. If the vapour transfer is not considered, the position of the ice lenses is between the 70 and 110 cm depth, which is close to the freezing front. The results indicate that a considerable deviation will occur if the vapour transfer is neglected.

4 Conclusions

This study presents a new model to describe frost heave in coarse-grained soils. The main feature of this model is taking into account vapour flow, which is usually neglected in previous studies. The proposed model is developed into an updated program PCHeave. A one-dimensional freezing experiment is used to evaluate the performance of the proposed model. The predicted results of frost heave and frost depth show good agreement with the measured values of laboratory experiments. The proposed model can reasonably reflect the process of frost heave in coarse-grained soils.

When applying the proposed model to simulate the frost heave in the coarse fills of a high-speed railway, the prediction of the model reasonably agrees with the measured

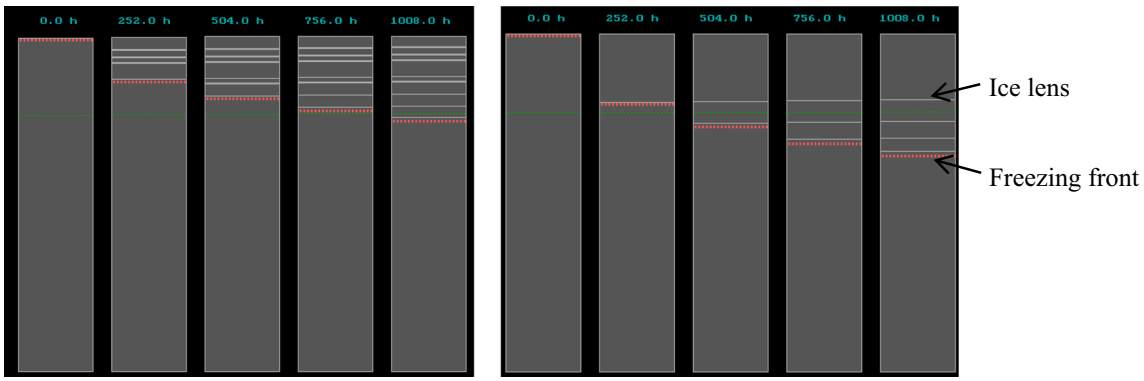

(a) considering vapour transfer **(b)** without considering vapour transfer

Fig. 9 Simulated ice lens formation in subgrade at site K1004

frost heave and frost depth over a relatively long period. The predicted frost heave has a relatively poorer match at the beginning of winter, which may be caused by the assumed boundary temperatures and overburden pressure. The simulated ice lenses are mainly distributed in the top 70 cm, which is in accordance with the monitored result that frost heave mainly occurs in the top 60 cm zone.

The computed results by the original PCHeave that neglected vapour transfer are also provided to make a comparison. It shows that the predicted frost heave without considering vapour flow is approximately 60% less than the measured data, and the predicted frost depth seems always deeper than the measured data. It also highlights that the contribution of vapour flow to the frost heave of coarse-grained soil is significant and cannot be neglected.

The updated PCHeave program does not require too many input parameters for boundary and material properties, and it is very simple to use and is computationally extremely fast. The proposed model provides a way to investigate frost heave in coarse-grained soils.

Acknowledgements This research was supported by the National Natural Science Foundation of China (Nos. 51878665, 51722812, and U1834206), and Innovation-Driven Project of Central South University (No. 2020CX034).

References

1. Beskow G (1935) Soil freezing and frost heaving with special application to roads and railroads. Swed Geol Surv Yearb 26(3), Series C, No. 375 (in Swedish)
2. Bronfenbrener L, Bronfenbrener R (2010) Modeling frost heave in freezing soils. Cold Reg Sci Technol 61:43–64
3. Cass A, Campbell GS, Jones TL (1984) Enhancement of thermal water vapor diffusion in soil. Soil Sci Soc Am J 48(1):25–32
4. Dash JG, Rempel AW, Wettlaufer JS (2006) The physics of premelted ice and its geophysical consequences. Rev Mod Phys 78(3):695–741
5. Eigenbrod KD, Kennepohl GJA (1996) Moisture accumulation and pore water pressures at base of pavements. Transp Res Rec 1546:151–161
6. Everett DH (1961) The thermodynamics of frost damage to porous solids. Trans Faraday Soc 57:1541–1551. https://doi.org/10.1039/tf9615701541
7. Farouki OT (1986) Thermal properties of soils. Trans Tech Publication, Clausthal-Zellerfeld
8. Fredlund DG, Rahardjo H (1993) Soil mechanics for unsaturated soils. Wiley, New York
9. Gao J, Lai Y, Zhang M, Feng Z (2018) Experimental study on the water-heat-vapor behavior in a freezing coarse-grained soil. Appl Therm Eng 128:956–965
10. Gilpin RR (1980) A model for the prediction of ice lensing and frost heave in soils. Water Resour Res 16(5):918–930
11. Guthrie WS, Hermansson Å, Woffinden KH (2006) Saturation of granular base material due to water vapor flow during freezing: laboratory experimentation and numerical modeling. Cold Reg Eng. https://doi.org/10.1061/40836(210)66
12. Hansson K, Simunek J, Mizoguchi M, Lundin LC, van Genuchten MT (2004) Water flow and heat transport in frozen soil: numerical solution and freeze-thaw applications. Vadose Zone J 3(2):693–704
13. Harlan RL (1973) Analysis of coupled heat-fluid transport in frozen soil. Water Resour Res 9(5):1314–1323
14. Jackson KA, Uhlmann DR, Chalmers B (1966) Frost heave in soils. J Appl Phys 37:848–852. https://doi.org/10.1063/1.1708270
15. Jame YW, Norum DI (1980) Heat and mass transfer in freezing unsaturated porous medium. Water Resour Res 16(4):811–819
16. Konrad JM, Morgenstern NR (1980) A mechanistic theory of ice lens formation in fine-grained soils. Can Geotech J 17(4):473–486
17. Konrad JM, Morgenstern JR (1981) The segregation potential of a freezing soil. Can Geotech J 18(4):482–491
18. Konrad JM, Morgenstern JR (1982) Effects of applied pressure on freezing soils. Can Geotech J 19(4):494–505
19. Konrad JM (2005) Estimation of the segregation potential of fine-grained soils using the frost heave response of two reference soils. Can Geotech J 42(1):38–50
20. Lai Y, Pei W, Zhang M, Zhou J (2014) Study on theory model of hydro-thermal-mechanical interaction process in saturated freezing silty soil. Int J Heat Mass Transf 78:805–819
21. Li S, Lai Y, Zhang M, Pei W, Zhang C, Yu F (2019) Centrifuge and numerical modeling of the frost heave mechanism of a cold-region canal. Acta Geotech 14:1113–1128
22. Liu Z, Yu X (2011) Coupled thermo-hydro-mechanical model for porous materials under frost action: theory and implementation. Acta Geotech 6:51–65
23. Liu H, Niu F, Niu Y, Lin Z, Lu J, Luo J (2012) Experimental and numerical investigation on temperature characteristics of high-speed railway's embankment in seasonal frozen regions. Cold Reg Sci Technol 81:55–64
24. Liu Q, Wang Z, Li Z, Wang Y (2019) Transversely isotropic frost heave modeling with heat-moisture-deformation coupling. Acta Geotech. https://doi.org/10.1007/s11440-019-00774-1
25. Miller RD (1972) Freezing and heaving of saturated and unsaturated soils. Highway Res Rec 393:1–11
26. Miller RD (1977) Lens initiation in secondary heaving. In: Proceedings of the international symposium on frost action in soils, Luleå University of Technology, Sweden, vol 2, pp 68-74
27. Miller RD (1978) Frost heaving in non-colloidal soils. In: Proceedings of the 3rd internal onal conference on permafrost, Edmonton, pp 708–713
28. Nakano Y (1997) A mathematical model called M_1 and the Gilpin model of soil freezing. In: Proceedings of the international symposium on ground freezing and frost action in soils, Lulea, pp 139–146
29. Niu F, Li A, Luo J, Lin Z, Yin G, Liu M, Zheng H, Liu H (2017) Soil moisture, ground temperatures, and deformation of a high-speed railway embankment in Northeast China. Cold Reg Sci Technol 133:7–14
30. Niu F, Zheng H, Li A (2020) The study of frost heave mechanism of high-speed railway foundation by field-monitored data and indoor verification experiment. Acta Geotech 15:581–593
31. Nixon JFD (1991) Discrete ice lens theory for frost heave in soils. Can Geotech J 28(8):843–859
32. Nyameogo GFT, Mbonimpa M, Bussière B, Awoh A (2020) Influence of frozen conditions on the oxygen diffusion coefficient in unsaturated porous materials. Acta Geotech 15:409–421
33. O'neill K, Miller RD (1985) Exploration of a rigid ice model of frost heave. Water Resour Res 21(5):281–296
34. Or D, Lehmann P, Shahraeeni E, Shokri N (2013) Advances in soil evaporation physics—a review. Vadose Zone J 12(4):vzj2012.0163
35. Philip JR, de Vries DA (1957) Moisture movement in porous materials under temperature gradients. Trans Am Geophys Union 38(2):222–232

36. Rempel AW, Wettlaufer JS, Worster MG (2004) Premelting dynamics in a continuum model of frost heave. J Fluid Mech 498:227–244
37. Rempel AW (2007) Formation of ice lenses and frost heave. J Geophys Res 112(F2):F02S21. https://doi.org/10.1029/2006jf000525
38. Rempel AW (2010) Frost heave. J Glaciol 56(200):1122–1128
39. Ren X, Kang J, Ren J, Chen X, Zhang M (2020) A method for estimating soil water characteristic curve with limited experimental data. Geoderma 360:114013
40. Saito H, Šimunek J, Mohanty BP (2006) Numerical analysis of coupled water, vapor, and heat transport in the vadose zone. Vadose Zone J 5(2):784–800
41. Saruya T, Kurita K, Rempel A (2013) Experimental constraints on the kinetics of ice lens initiation and growth. Phys Rev E 87:032404
42. Sheng D (1994) Thermodynamics of freezing soils, theory and application. (Doctoral Dissertation) Luleå University of Technology, Sweden (1994: 141D)
43. Sheng D, Axelsson K, Knutsson S (1995) Frost heave due to ice lens formation in freezing soils: 1. Theory and verification. Nord Hydrol 26(2):125–146
44. Sheng D, Axelsson K, Knutsson S (1995) Frost heave due to ice lens formation in freezing soils: 2. Field application. Nord Hydrol 26(2):147–168
45. Sheng D, Zhang S, Yu Z, Zhang J (2013) Assessing frost susceptibility of soils using PCHeave. Cold Reg Sci Technol 95:27–38
46. Sheng D, Zhang S, Niu F, Cheng G (2014) A potential new frost heave mechanism in high-speed railway embankments. Géotechnique 64(2):144–154
47. Taber S (1930) The mechanics of frost heaving. J Geol 37:303–317
48. Teng J, Yasufuku N, Zhang S, He Y (2016) Modelling water content redistribution during evaporation from sandy soil in presence of water table. Comput Geotech 75:210–224
49. Teng J, Zhang X, Zhang S, Zhao C, Sheng D (2019) An analytical model for evaporation from unsaturated soil. Comput Geotech 108:107–116
50. Teng J, Shan F, He Z, Zhang S, Zhao G, Sheng D (2019) Experimental study of ice accumulation in unsaturated clean sand. Géotechnique 69(3):251–259
51. Teng J, Kou J, Zhang S, Sheng D (2019) Evaluating the influence of specimen preparation on saturated hydraulic conductivity using nuclear magnetic resonance technology. Vadose Zone J 18:180179
52. Teng J, Kou J, Yan X, Zhang S, Sheng D (2020) Parameterization of soil freezing characteristic curve for unsaturated soils. Cold Reg Sci Technol 70:102928
53. Thomas HR, Cleall P, Li Y, Harris C, Kern-Luetschg M (2009) Modelling of cryogenic processes in permafrost and seasonally frozen soils. Géotechnique 59(3):173–184
54. Yao Y, Wang L (2019) Double pot cover effect in unsaturated soils. Acta Geotech 14:1037–1047
55. Zhang S, Sheng D, Zhao G, Niu F, He Z (2016) Analysis of frost heave mechanisms in a high-speed railway embankment. Can Geotech J 53(3):520–529
56. Zhang S, Teng J, He Z, Liu Y, Liang S, Yao Y, Sheng D (2016) Canopy effect caused by vapour transfer in covered freezing soils. Géotechnique 66(11):927–940
57. Zhang S, Teng J, He Z, Sheng D (2016) Importance of vapor flow in unsaturated freezing soil: a numerical study. Cold Reg Sci Technol 126:1–9